Brownian Dynamics Model of Excited-State Relaxation in Solutions of Conjugated Oligomers

Nicolae M. Albu and David J. Yaron*.

Department of Chemistry, Carnegie Mellon University, 4400 Fifth Avenue, Pittsburgh, Pennsylvania 15213.

Excited state relaxation, conjugated polymers, Brownian dynamics.

The effects of torsional degrees of freedom on the excited-state relaxation of conjugated oligomers in solution are explored computationally by coupling an exciton model of the oligomer to a Brownian dynamics model of the solvent. The exciton model assigns one torsional degree of freedom to each unit cell, or site, of the oligomer. A simple molecular mechanical form is used for the ground electronic state. The excitation energy is obtained assuming coherent coupling between sites that is proportional to the cosine of the difference in torsional angles. The solvent is characterized by a single parameter, which is equivalent to setting the rotational diffusion time, t_{rot}, of a single unit cell about the oligomer axis in the absence of any internal forces. The relaxation of long oligomers exhibits a fast component, with a time constant that is about 0.025 t_{rot} and a slow component that is about 0.15 t_{rot}. As the oligomer length is decreased, the time constant for the slow component decreases such that the bi-exponential behavior smoothly diminishes below 10 unit cells, nearly disappearing by 3 unit cells. Comparisons of the

exciton model, which includes self-trapping, with molecular mechanics and harmonic oscillator models, which do not include self-trapping, show similar behaviors. The double exponential behavior therefore appears to be a general consequence of the participation of many torsional degrees of freedom in establishing the excitation energy. Since the time scales are relatively independent of the details of the torsional potential, experimental measurements of relaxation due to planarization report primarily on t_{rot}.

1. Introduction

Conjugated polymers have torsional degrees of freedom that are typically quite floppy. These degrees of freedom are an essential feature of the material, since they impart the flexibility required for the materials to be soluble and processable. These floppy degrees of freedom also lead to structural disorder, which plays a central role in the photophysics by establishing, for instance, spectral line shapes[1–4] and wavefunction localization.[5,6] Here, we explore the effects of torsional relaxation on the time-evolution of the first excited state for conjugated oligomers in solution. By using a relatively simple model for the electronic excitation and Brownian dynamics to include the effects of solvent, we can obtain converged ensemble averages of the relaxation behavior. Of particular interest is the bi-exponential nature of the time evolution, and the factors that influence the relaxation time scales.

The model explored here focuses on the planarization of an oligomer due to the presence of the excitation. This planarization results from an increase in the torsional potential upon photo-excitation, and contributes to the spectral relaxation in the tens of ps time range.[4,7–18] On longer oligomers, this leads to self-trapping of the excitation onto a localized, planarized, region.[5,6] The effects of the self-trapping on the time dynamics are explored by comparing results obtained

from an exciton model, that includes self-trapping, with simpler models in which self-trapping does not occur. The model focuses on only the planarization in the lowest excited state, and ignores other effects that influence the spectral relaxation. The formation of exciton-polarons due to stretching degrees of freedom is expected to occur on a much faster time scale than the torsional relaxation[19,20] and is not included. Hopping of the excitation between different localized regions on the same polymer chain and between adjacent chains is also not included, and such phenomena may occur with time scales that are similar to those from the planarization explored here.[21–23] The ultrafast relaxation that arises from non-adiabatic electronic relaxation, which has recently been shown to occur from highly-excited electronic states[24] is also not included.

Section 2 discusses the models used for both the excitation energy and the Brownian dynamics. Section 3 discussed the data generation and the fitting used to extract time constants from the dynamics trajectories. Section 4 presents the results, following by concluding comments in Section 5.

2. Model

Exciton (EX) Model

We begin by considering an Exciton model (EX), which views the excited state as containing an exciton that hops coherently between generalized sites (unit cells) of an oligomer. We then consider simplifications that remove self-trapping effects and nonlinearity of the torsional potential. In the EX model, each site has a single torsional degree of freedom, θ_i, as shown in

Figure 1. The torsional potential in the ground state is modeled with a simple molecular mechanical form, written as:

$$E_{gs} = \frac{1}{2} V_{gs} \sum_{i=1}^{N-1} \left[1 - \cos\left[2(\theta_{i+1} - \theta_i) \right] \right] \qquad (1)$$

where θ_i is the angle of the ith ring, and V_{gs} is the magnitude of the torsional potential. This is the lowest order trigonometric form that has a minimum for the planar structure and a maximum for all rings twisted to 90 degrees.

The excited state model assumes that the exciton hops coherently between sites, with a coupling term that depends on the angle between the adjacent rings, $\beta_{es} \cos(\theta_{i+1} - \theta_i)$, as shown in Figure 1. The excitation energy is modeled as the lowest eigenvalue of the following Hamiltonian.

$$\begin{pmatrix} \alpha & \beta_{es} \cos(\theta_2 - \theta_1) & 0 & \cdots & 0 & 0 \\ \beta_{es} \cos(\theta_2 - \theta_1) & \alpha & \beta_{es} \cos(\theta_3 - \theta_2) & \cdots & 0 & 0 \\ 0 & \beta_{es} \cos(\theta_3 - \theta_2) & \alpha & \cdots & 0 & 0 \\ \cdots & \cdots & \cdots & \cdots & \cdots & \cdots \\ 0 & 0 & 0 & \cdots & \alpha & \beta_{es} \cos(\theta_N - \theta_{N-1}) \\ 0 & 0 & 0 & \cdots & \beta_{es} \cos(\theta_N - \theta_{N-1}) & \alpha \end{pmatrix} (2)$$

The form $\beta_{es} \cos(\theta_{i+1} - \theta_i)$ was obtained from fits of the above model to INDO calculations, on a series of poly-phenyleneethynylene (PPE) oligomers with varying chain lengths and dihedral angles.[25] The total energy of the excited state, $E_{es,}$ is the sum of the ground state energy of Eq. (1) and the lowest eigenvalue of Eq. (2).

This model includes self-trapping of the exciton on a region of the polymer chain, due to planarization of the oligomer in the vicinity of the exciton. Since stretching degrees of freedom are not included in the model, the additional self-trapping expected from C-C stretches is not included.[2,20,26] The time scale associated with self-trapping from C-C stretches is sub-picosecond, and occurs much more rapidly than the planarization of the oligomer, which is the target of this work.[19,27]

Results are shown below for V_{gs} of Eq. (1) having values between 0 and 6 kcal/mol, based on the range expected for conjugated polymers (2.3 kcal/mol for poly-paraphenylenevinylene, PPV[28], 2.3 kcal/mol for poly-fluorene, PF[8], and 0.6 kcal/mol for poly-phenyleneethynylene, PPE[1], ~9 kcal/mol for poly-thiophene, PT[29,30]). The excited state coupling, β_{es}, establishes the exciton band width. We compare results for β_{es} = -10, -20, and -30 kcal/mol, which also spans the range expected for conjugated oligomers.

Molecular-Mechanics (MM) Model

In the above EX model, the presence of the exciton increases the torsional potential in the vicinity of the exciton, and leads to self-trapping onto a planarized region of the oligomer. To isolate the effects of self-trapping, we compare results to those obtained with a molecular-mechanics (MM) model that treats the excitation as increasing the torsional potential uniformly across the oligomer. This is done by using the following molecular mechanics form for the excitation energy:

$$E_{es} = E_{es-planar} + \frac{1}{2} V_{es} \sum_{i=1}^{N-1} \left[1 - \cos\left[2\left(\theta_{i+1} - \theta_i \right) \right] \right] \qquad (3)$$

where $E_{es\text{-}planar}$ is the excitation energy of a planar oligomer. The torsional potential has the same form as the ground state of Eq. (1) but with a different barrier, V_{es}. The value of $E_{es\text{-}planar}$ has no effect on the time dynamics explored below. Results are shown for values of V_{es} between 0.6 and 6.0 kcal/mol. These were chosen to be roughly equivalent to the excited state torsional potential resulting from the values of β_{es} used in the EX model. However, it is not possible to choose a value of V_{es} that would map onto a given β_{es} for all chain lengths. Consider the effect on the excitation energy of twisting the chain such that all torsional angles are 90 degrees. For long chains within the EX model, such twisting raises the excitation energy by $2\,|\beta_{es}|$. Within the MM model, such twisting raises the energy by an amount, $(N\text{-}1)(V_{es} - V_{gs})$, which does not saturate with increasing chain length. For these to agree on an oligomer with length N, V_{es} of the MM model should be about $|\beta_{es}|/N$. This difference in behavior with chain length reflects the lack of self-trapping in the MM model. In the EX model, as the exciton localizes, the torsional barrier increases only in the vicinity of the exciton, such that the excitation energy has the correct behavior of saturating with chain length. We consider V_{es} values from 0.6 to 6 kcal/mol, to cover the range corresponding to oligomers with length 5 to 10 for β_{es} from -10 to -30 kcal/mol.

Harmonic Model

To further simplify the model, we replace the cosine potentials of Eqs. (1) and (3) with a harmonic potential, creating a Harmonic Oscillator model (HO). The excitation energy in the HO model is

$$E_{es} = E_{es-planar} + \frac{V_{es}}{(\pi/2)^2} \sum_{i=1}^{N-1}\left[(\theta_{i+1}-\theta_i)^2\right] \quad (4)$$

where V_{es} is the energy associated with twisting one inter-ring angle of the oligomer from 0 to 90 degrees. The range of V_{es} is thus the same as used above for the MM model. Comparison with the MM model thus explores the effects of nonlinearity in the torsional forces on the time dynamics.

Brownian Dynamics

To model planarization of conjugated oligomers in solution, we use Brownian dynamics to include solvent effects. In Brownian dynamics, the solvent gives rise to both stochastic forces and friction, via the following[31]

$$\dot{\theta}_i = v_i$$
$$\dot{v}_i = a_i - \gamma v_i + A_i \quad (5)$$

where θ_i and v_i are the torsional angle and velocity, respectively, of the ith unit cell, and a_i is the acceleration due to forces calculated as analytical derivatives of the torsional potentials described above,

$$a_i = \frac{1}{I}\frac{dE}{d\theta_i} \quad (6)$$

Here I is the moment of inertia of a ring, taken as the polythiophene (PT) value of *91.1 amu·Å²*. The friction coefficient, γ in Eq. (5), is the same for all sites, which assumes that the solvent effects are isotropic and independent of the system configuration. Finally, the random force term, $A_i(t)$ of Eq. (5), is a stochastic Gaussian process given by:

$$
\begin{aligned}
\left\langle A_i(t) \right\rangle &= 0 \\
\left\langle A_i(t) A_j(0) \right\rangle &= \delta_{ij} \cdot 2\gamma \frac{k_B T}{I} \cdot \delta(t)
\end{aligned}
\qquad (7)
$$

The random force in Eq. (7) is related to the solvent friction by the fluctuation-dissipation theorem, such that the model contains only one parameter, γ, which defines the nature of the solvent. Rather than quote the value of γ below, we quote the rotational diffusion time, t_{rot}, of a single unit cell that arises from the solvent in the absence of any intra-molecular forces. Note that this is the diffusion time for rotation of a unit cell about the polymer axis, as opposed to the rotational diffusion time of a free unit cell in solution. The relation between γ and t_{rot} is linear, as shown in Figure 2. Below, we compare results for t_{rot} of 7.5 and 225 ps.

3. Computational methods

Data Generation

For each model and set of parameters, 10,000 trajectories were run and the excitation energy as a function of time was averaged. Each trajectory has an equilibration phase of 200 time steps, in which the torsional potential is that of the ground state. In this equilibration phase, the time step is 48.9 fs for t_{rot} = 7.5ps and 146.7 fs for t_{rot} = 225 ps. This is followed by a relaxation phase of

1500 time steps, in which the potential is that of the excited state. In the relaxation phase, the time step is one tenth that of the equilibration phase. Decreasing the above time steps by a factor of 5, while keeping the total time the same, leads to relaxation time constants in agreement to within 2% of those obtained with the larger time step, as shown in Table 1.

Data Fitting

The excitation energy is averaged over 10,000 trajectories, to give an ensemble average of excitation energy versus time. This is then fit to extract time constants for the relaxation of the excitation energy. Relaxation on chains with 3 or more unit cells involves two distinct time scales. Figure 3 shows typical results for all three models. The black circles are the ensemble averaged relaxation data (raw data), with time 0 being the point at which the excitation occurs. Fits are shown to both single and double exponential forms. In all three models, the double exponential form leads to a substantially better fit, indicating that there are two discernible time scales in the data.

For chains with only two unit cells ($N=2$), the relaxation behavior is not well described by exponential decay forms. Results for $N=2$ are discussed in Section 4 regarding memory effects, but are otherwise not included in the discussion.

4. Results

Exciton delocalization

The models considered here include only torsional degrees of freedom. Inclusion of stretching degrees of freedom will lead to formation of exciton-polarons. Formation of such exciton-polarons is expected to occur in tens of femtoseconds, after which the relaxation is dominated by the slower torsional degrees of freedom considered here.[19] However, in addition to an ultrafast component to the relaxation, exciton-polaron formation also contributes to self-localization of the exciton. In the EX model, localization arises only from disorder in the torsional degrees of freedom.

Figure 4 shows the localization length of the excitons within the EX model, as defined by the participation ratio.[5,6] As the magnitude of β_{es} increases from -10 to -30 kcal/mol, the localization increases from 8 to nearly 14. For β_{es} of -30 kcal/mol, the localization length may be larger than is reasonable for an exciton-polaron and this may limit the reliability of the EX model.

Memory Effects

To better understand the nature of the dynamics, we consider memory effects in the relaxation. By memory, we mean the degree to which future relaxation depends on the past history. Figure 5 shows results for chain lengths of $N=2$ (upper panels) and $N=10$ (lower panels) for the three models discussed in Section 2. Consider first the EX model with chain length $N=2$. Three trajectories are shown, which have different ground state potentials but the same excited state coupling, β_{es} = -30kcal/mol. Since the excited-state relaxation begins with an ensemble equilibrated to the ground state potential, the three trajectories start with different degrees of planarity. Since the excited state coupling dominates the excited-state potential, all three trajectories are relaxing to nearly the same final ensemble. The relaxation is monitored through

the excitation energy, which is related to the average torsional angle of the system. The trajectory, Energy(t), for which $V_{gs} = 0.6$ kcal/mol starts furthest from planarity, and by 0.06 ps has relaxed to a point where the average energy is equal to the starting energy of the trajectory for which $V_{gs} = 1.5$ kcal/mol. In Figure 5, the $V_{gs} = 1.5$ kcal/mol trajectory has been shifted by 0.06 ps, such that if there were no memory effects, the two trajectories would superimpose. The deviation is such that the trajectory that started further from equilibrium relaxes more rapidly towards equilibrium. This is as expected for inertial behavior, since the trajectory that started further from equilibrium has picked up momentum. A similar displacement of the $V_{gs} = 2.5$ kcal/mol trajectory shows the same type of memory effect.

The opposite behavior is seen for chains with length $N=10$, as shown in the lower left panel of Figure 5 for the EX model. In this case, the trajectory that starts further from equilibrium relaxes more slowly towards equilibrium. The factors that contribute to this can be explored by comparison with the other models. For $N=2$ within the MM and HO model, the memory effects are more complex. Trajectories that start closer to the equilibrium state initially relax slower and then catch up and surpass trajectories that start further from equilibrium. (This crossing of trajectories is more visible in Figure 5 for the HO model, but is also present in the MM model.) From this, we can conclude that, for $N=2$, the inertial memory effect seen within the EX model results from the particular form of the excited state potential within the EX model. For longer chains, similar memory effects are seen for all three models. This indicates that the memory effects on longer chains is a result of having multiple torsional degrees of freedom and is not sensitive to the particular form of the excited state potential. Below, we will show that as chain length increases, the slow component of the relaxation plays an increasing important role. The

presence of a slow exponential component is able to account for the type of memory effects seen on long chains.

Chain Length Dependence of the Relaxation

Figure 6 through Figure 8 show results from double exponential fits to the energy relaxation obtained from each of the models, for various parameter choices. Some common behaviors are seen across all models and parameters. On long chains, a slow relaxation component is observed with a time constant that is approximately an order of magnitude larger than the fast component. The relative amplitude of this component is substantial, approximately 40% for the EX model and 20% for the MM and HO models, such that the slow component dominates the relaxation behavior at long times. As one moves to shorter chains, the time constant of the fast component remains roughly constant, while that of the slow component approaches that of the former. The decrease in the time constant of the slow component with decreasing chain length is similar across all three models, suggesting that this phenomenon arises from averaging over multiple torsional degrees of freedom, and is independent of the specific nature of the excited state potential. The time constant of the slow component becomes roughly constant beyond chain lengths of about 10, which is comparable to the delocalization length. However, since only the EX model includes self-trapping of the excitation onto a region of the chain, and similar behaviors are seen across all three models, the presence and behavior of the slow component is not related to self-trapping and instead must arise solely from averaging across multiple degrees of freedom. The slow component is also not due to slow cooling, since the temperature derived

from the average kinetic energy of the torsional degrees of freedom of the oligomer returns to room temperature quickly following excitation (data not shown).

Some differences between the EX and the MM and HO model are apparent in the amplitudes of the slow component, shown in the lower panels of Figure 6 through Figure 8. On long chains, the relative magnitude of the slow component in the EX model is roughly twice that seen in the MM and HO models. In addition, as one moves to shorter chains, the MM and HO model predict substantial increases in the relative amplitude of the slow component. A similar effect is not seen in the EX model, although we note that the relative amplitude of the slow component within the EX model becomes noisy on short chains. This noise may reflect difficulties associated with resolving relaxation components with similar time constants. In addition, since systems with 2 rings do not exhibit exponential decay behavior, this noise may also reflect dynamics on short chains that are not well described by a bi-exponential form. Nevertheless, the results clearly indicate that as chain length is increased, a slow component appears in the relaxation behavior.

Figure 7 shows the effects of altering the ground-state potential, while keeping the excited-state potential fixed. In all cases, changes in the excited state potential have a larger effect on the slow component than on the fast component, with the effect on the fast component being negligible in the EX model. In the EX model, the slow component becomes somewhat faster as the ground-state potential is increased. The opposite behavior is seen in the MM and HO models. However, in all cases, the effects of the potential on the time constants are relatively small.

Figure 8 shows the results obtained when the rotational diffusion time of a single ring, t_{rot} of Figure 6, is increase by a factor 30 to 225 ps. Comparison with Figure 6 reveals that the time constants of both the slow and fast components increase by roughly a factor of 30, while the relative amplitude of the slow component remains about the same. The time constants are thus

roughly proportional to t_{rot}. The simulation results therefore provide the expected time constants for the excited-state relaxation as multiples of t_{rot}, where t_{rot} characterizes the effects of the solvent on the rotational dynamics of a single ring. A range of 10 to 300 ps for t_{rot}, as may be reasonable for oligomers with varying types of side chains and in various solvents, leads to a predicted range of about 1.5 to 45 ps for the slow component, with the fast component being about six times faster (0.25 ps to 7.5 ps). The predicted slow component is consistent with the 10's of ps relaxation components that have been attributed to torsional degrees of freedom.[4,7–18]

5. Conclusions

The simulations performed here examine the contribution of torsional degrees of freedom to the excited-state relaxation of conjugated oligomers. The use of a relatively simple model for the excitation energy allows extensive ensemble averaging, such that the presence of two time scales can be discerned in the relaxation behavior of long oligomers. The model contains a single parameter that characterizes the solvent, and this parameter can be viewed as setting the rotational diffusion time, t_{rot}, of a single polymer unit cell about the polymer axis in the absence of any internal forces. The relaxation of long oligomers exhibits a fast component, with a time constant that is about 0.025 t_{rot} and a slow component that is about 0.15 t_{rot}. As the oligomer length is decreased, the time constant for the slow component decreases such that the bi-exponential behavior smoothly diminishes below 10 unit cells, nearly disappearing by 3 unit cells. (For 2 unit cells, the behavior is not well described by single or double exponential forms). Comparisons of an exciton model, which includes self-trapping, with molecular mechanics and harmonic oscillator models, which do not include self-trapping, show similar behaviors. Likewise, the behavior is not strongly dependent on the parameters that define the strength of the

ground and excited state torsional potentials. The double exponential behavior therefore appears to be a general consequence of the participation of many torsional degrees of freedom in establishing the excitation energy. Since the time scales are relatively independent of the details of the torsional potential, experimental measurements of relaxation due to planarization report primarily on t_{rot}, the rotational diffusion time of a single ring about the polymer axis. Assuming the 10 to 40 ps relaxation times[4,7–18] attributed to torsion relaxation correspond to the slow (0.15 t_{rot}) component, this suggests t_{rot} of these systems is in the range 60 to 250 ps.
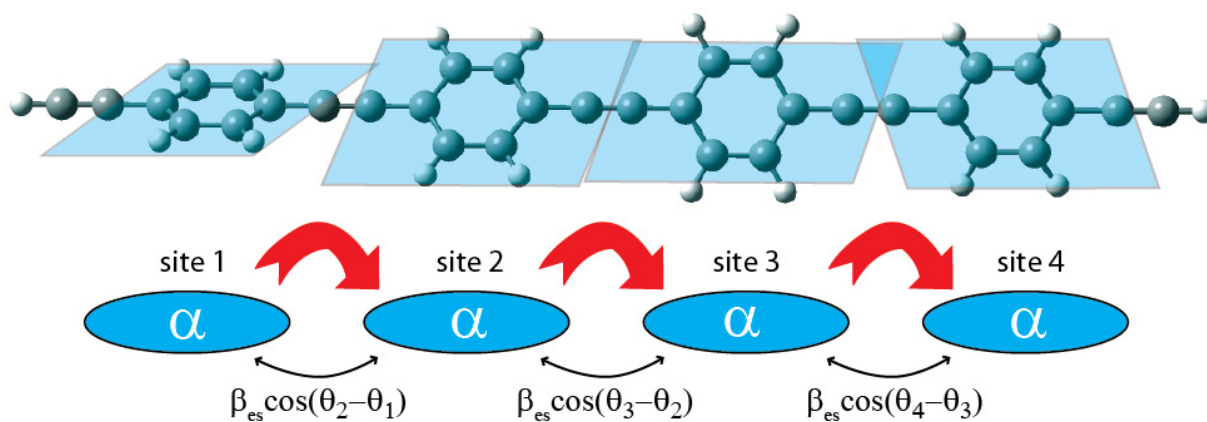
Figure 1. Schematic representation of the exciton model used for the excited states. Each unit cell is a site with energy α, with coupling between sites as shown.
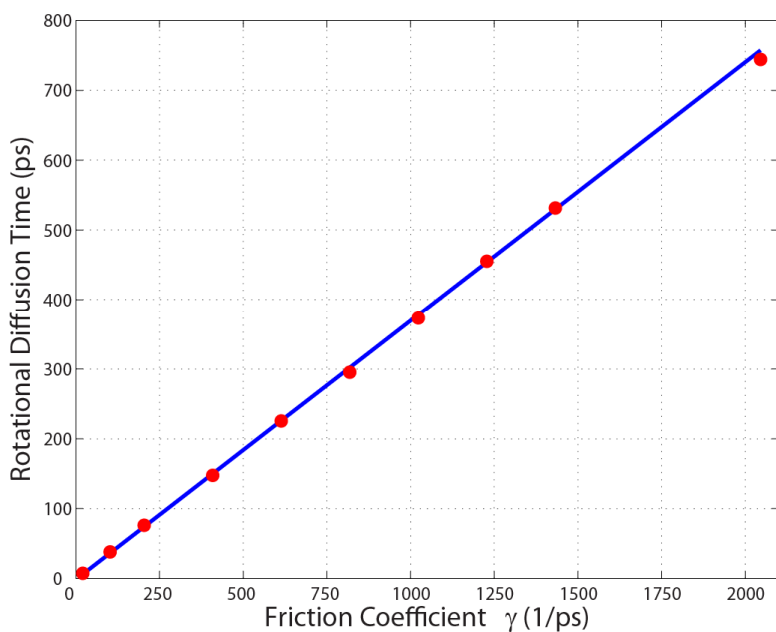
Figure 2. Linear dependency of the rotational diffusion time of a single ring versus the friction coefficient of Eq. (5).
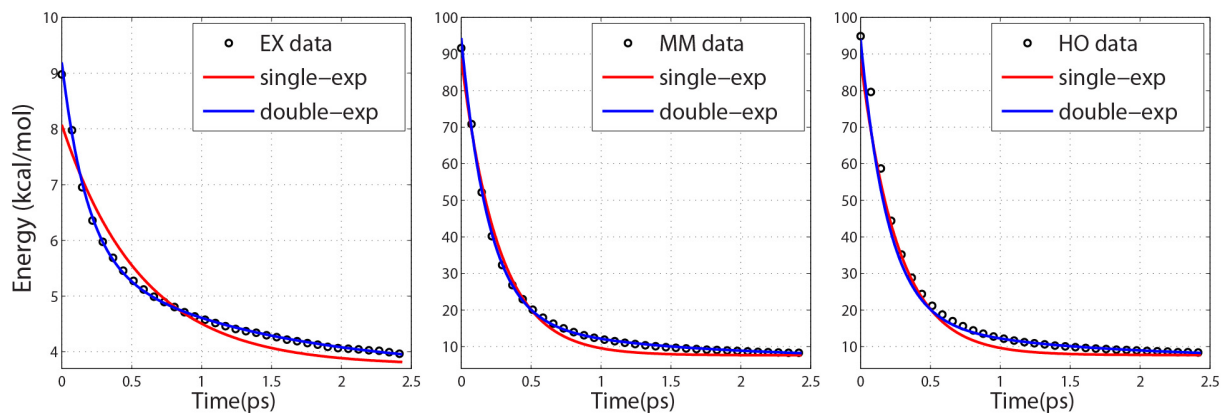
Figure 3. Fits of relaxation data to single and double exponentials. The simulations are for $N=20$ and $t_{rot} = 7.5$ ps, with potentials: EX model (left) $V_{gs} = 0.6$ kcal/mol, $\beta_{es} = -30$ kcal/mol; MM model (center) $V_{gs} = 0$ and $V_{es} = 6$ kcal/mol; HO model (right) $V_{gs} = 0$ and $V_{es} = 6$ kcal/mol.
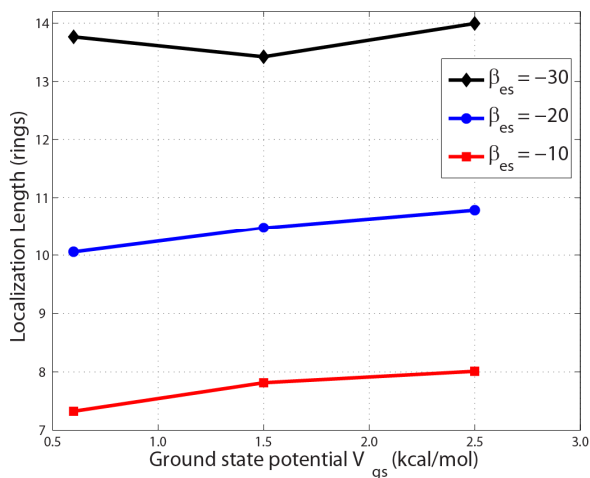

Figure 4. Localization length as a function of the ground state potential, V_{gs}.
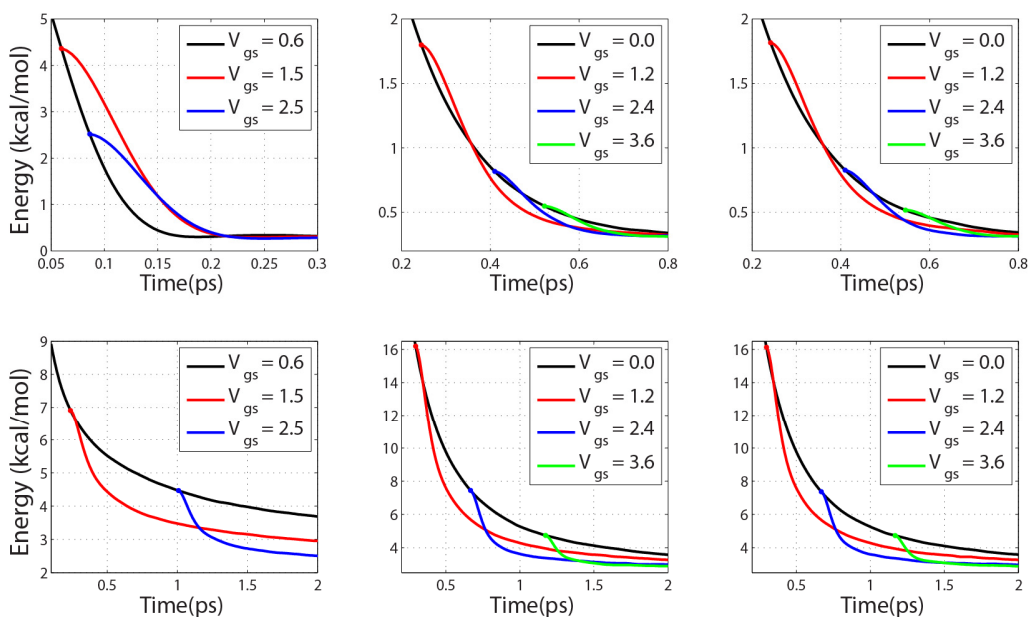
Figure 5. Memory effects for the EX model (left), the MM model (middle), and the HO model (right). The upper panels are for a chain length of 2. The lower panels are for a chain lengths of 10. The ground state potential is as shown in the legend. In the EX model, the excited state coupling, β_{es}, is fixed at -30 kcal/mol. For the MM and HO models, the excited state potential is fixed at 6 kcal/mol.
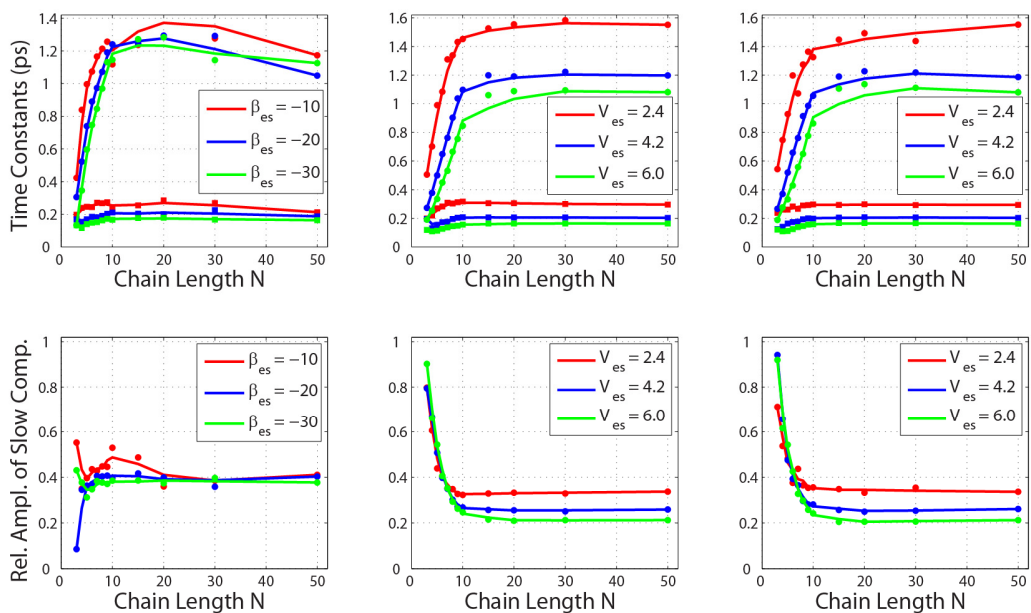
Figure 6. Dependence on excited-state potential. The time constants (upper) and relative amplitude of the slow component (lower) are shown for the EX (left), MM (middle), and HO (right) models. The ground state potential is fixed at 0.6 kcal/mol for all three models, and the excited state potential is as shown in the legends. t_{rot} is 7.5 ps. The lines are smoothed curves, obtained by averaging with a window of 3.
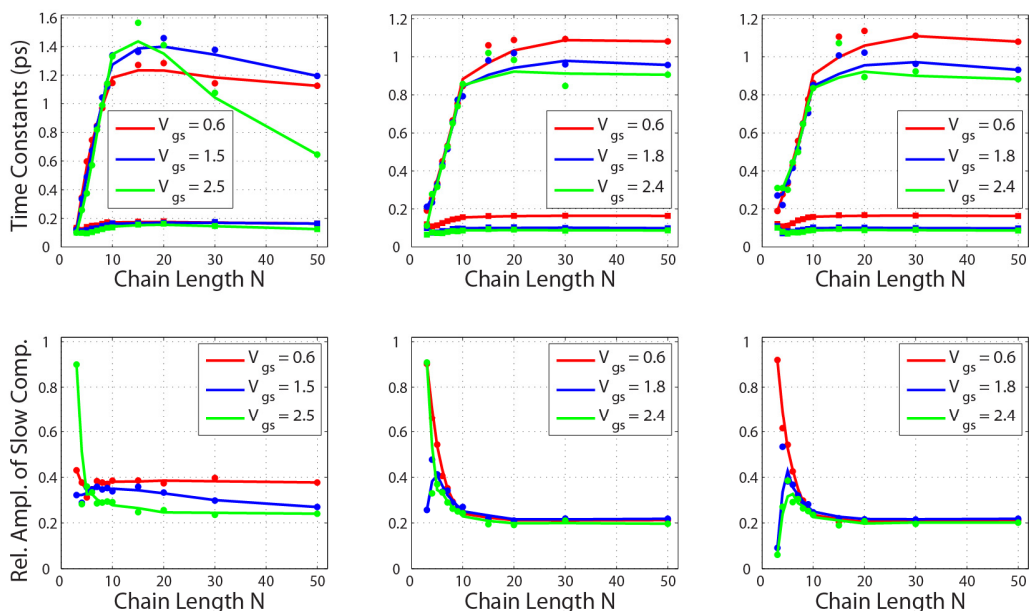
Figure 7. Dependence on ground-state potential. Time constants (upper) and relative amplitude of the slow component (lower) are shown for the EX (left), MM (middle), and HO (right) models. The excited state potential is fixed at β_{es} of -30 kcal/mol for the EX model and $V_{es} = 6$ kcal/mol for the MM and HO models, with V_{gs} as shown in the legends. t_{rot} is 7.5ps. The lines are smoothed curves, obtained by averaging with a window of 3.
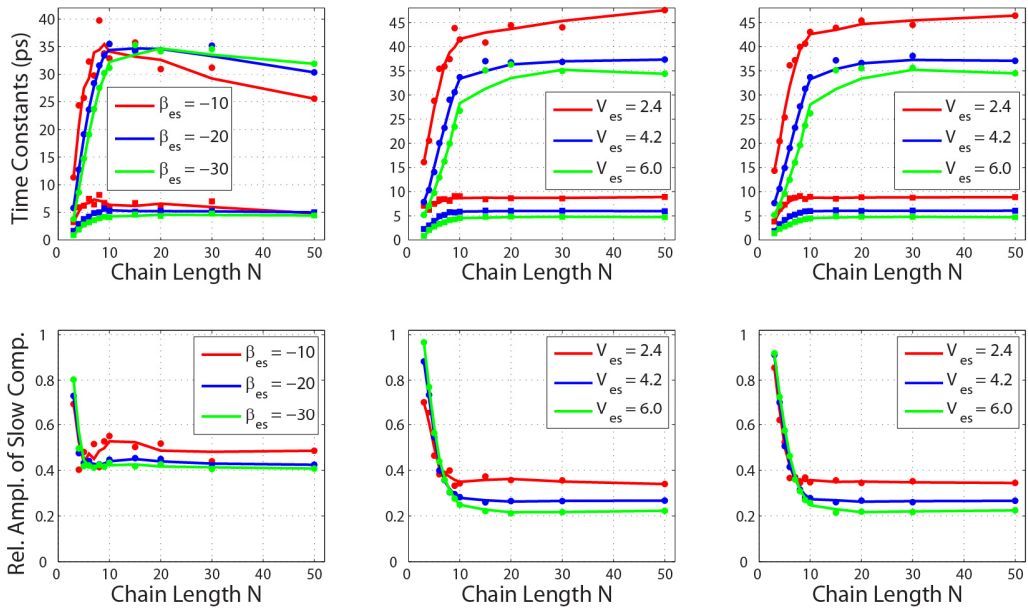
Figure 8. Dependence on rotational diffusion time of a single ring. Simulation parameters and plotting conventions are the same as Figure 6, with the exception that t_{rot} is 225 ps here (30 times the value used in Figure 6). The results indicate the time constants are roughly proportional to t_{rot}.

Table 1. Comparison of relaxation times as a function of integration time step, for an oligomer with 20 unit cells and with t_{rot} = 7.5 ps. For the MM model V_{gs} = 0 and V_{es} = 6 kcal/mol. For EX model V_{gs} = 0.6 kcal/mol and β_{es} = -30 kcal/mol. Results from fits to single exponential (τ_{1-1}) and a double exponential (τ_{2-1}, τ_{2-2}) forms are shown.

Model	Time Step	τ_{1-1}	τ_{2-1}	τ_{2-2}
EX	0.02	0.5802	0.1766	1.2687
	0.10	0.5716	0.1791	1.2835
MM	0.02	0.2676	0.1950	1.2402
	0.10	0.2667	0.1944	1.2177

REFERENCES

(1)   Liu, L. T.; Yaron, D.; Berg, M. A. *Journal of Physical Chemistry C* **2007**, *111*, 5770–5782.

(2)   Heimel, G.; Daghofer, M.; Gierschner, J.; List, E. J. W.; Grimsdale, A. C.; Müllen, K.; Beljonne, D.; Brédas, J.-L.; Zojer, E. *The Journal of chemical physics* **2005**, *122*, 54501.

(3)   Becker, K.; Da E., C.; Feldmann, J.; Scheliga, F.; Thorn E., C.; Tretiak, S.; Lupton, J. M. *Journal of Physical Chemistry B* **2008**, *112*, 4859–4864.

(4)   Dykstra, T. E.; Scholes, G. D. In *Ultrafast Dyn. Laser Action Org. Semicond.*; CRC Press, 2009; pp. 169–201.

(5)   Barford, W.; Lidzey, D. G.; Makhov, D. V; Meijer, A. J. H. *The Journal of chemical physics* **2010**, *133*, 044504.

(6)   Barford, W.; Trembath, D. *Physical Review B* **2009**, *80*, 165418.

(7)   Westenhoff, S.; Beenken, W. J. D.; Friend, R. H.; Greenham, N. C.; Yartsev, A.; Sundstrom, V. *Physical review letters* **2006**, *97*, 166804.

(8)   Chen, H. L.; Huang, Y. F.; Lim, T. S.; Su, C. H.; Chen, P. H.; Su, A. C.; Wong, K. T.; Chao, T. C.; Chan, S. I.; Fann, W. *Journal of Physical Chemistry B* **2009**, *113*, 8527–8531.

(9)   Parkinson, P.; Muller, C.; Stingelin, N.; Johnston, M. B.; Herz, L. M. *Journal of Physical Chemistry Letters* **2010**, *1*, 2788–2792.

(10)   Banerji, N.; Cowan, S.; Vauthey, E.; Heeger, A. J. *Journal of Physical Chemistry C* **2011**, *115*, 9726–9739.

(11)   Yu, W.; Zhou, J.; Bragg, A. E. *Journal of Physical Chemistry Letters* **2012**, *3*, 1321–1328.

(12)   Busby, E.; Carroll, E. C.; Chinn, E. M.; Chang, L.; Moule, A. J.; Larsen, D. S. *Journal of Physical Chemistry Letters* **2011**, *2*, 2764–2769.

(13)   Fujitsuka, M.; Cho, D. W.; Huang, H.-H.; Yang, J.-S.; Majima, T. *Journal of Physical Chemistry B* **2011**, *115*, 13502–13507.

(14)   Hoffmann, S. T.; Bassler, H.; Kohler, A. *Journal of Physical Chemistry B* **2010**, *114*, 17037–17048.

(15)   Badaeva, E.; Harpham, M. R.; Guda, R.; Suzer, O.; Ma, C.-Q.; Bauerle, P.; Goodson, T.; Tretiak, S. *Journal of Physical Chemistry B* **2010**, *114*, 15808–15817.

(16)   Chang, M.-H.; Hoffmann, M.; Anderson, H. L.; Herz, L. M. *Journal of the American Chemical Society* **2008**, *130*, 10171–10178.

(17)   Wells, N. P.; Blank, D. A. *Physical Review Letters* **2008**, *100*, 086403/1–086403/4.

(18)   Sluch, M. I.; Godt, A.; Bunz, U. H. F.; Berg, M. A. *Journal of the American Chemical Society* **2001**, *123*, 6447–6448.

(19)   Barford, W.; Boczarow, I.; Wharram, T. *The journal of physical chemistry. A* **2011**, *115*, 9111–9.

(20)   Tretiak, S.; Saxena, A.; Martin, R. L.; Bishop, A. R. *Physical Review Letters* **2002**, *89*, 097402/1–097402/4.

(21)   Van Bernard, A.; Beljonne, D.; Van, A. B. *Journal of Physical Chemistry A* **2009**, *113*, 2677–2682.

(22)   Saini, S.; Bagchi, B. *Physical Chemistry Chemical Physics* **2010**, *12*, 7427–7433.

(23)   Singh, J.; Bittner, E. R.; Beljonne, D.; Scholes, G. D. *The Journal of chemical physics* **2009**, *131*, 194905.

(24)   Clark, J.; Nelson, T.; Tretiak, S.; Cirmi, G.; Lanzani, G. *Nature Physics* **2012**, *8*, 225–231.

(25)   Liu, L. T.; Yaron, D.; Sluch, M. I.; Berg, M. A. *The journal of physical chemistry. B* **2006**, *110*, 18844–52.

(26)   Nayyar, I. H.; Batista, E. R.; Tretiak, S.; Saxena, A.; Smith, D. L.; Martin, R. L. *The Journal of Physical Chemistry Letters* **2011**, *2*, 566–571.

(27)   Fernandez-Alberti, S.; Roitberg, A. E.; Kleiman, V. D.; Nelson, T.; Tretiak, S. *The Journal of chemical physics* **2012**, *137*, 22A526.

(28)   Hultell, M.; Stafstroem, S. *Physical Review B: Condensed Matter and Materials Physics* **2009**, *79*, 014302/1–014302/7.

(29)   Pan, J.-F.; Chua, S.-J.; Huang, W. *Chemical Physics Letters* **2002**, *363*, 18–24.

(30)   Darling, S. B. *Journal of Physical Chemistry B* **2008**, *112*, 8891–8895.

(31)   Allen, M. P. *Molecular Physics* **1980**, *40*, 1073–1087.